JOURNAL OF AGRICULTURAL AND FOOD CHEMISTRY

pubs.acs.org/JAFC Article

Highly Selective and Sensitive Detection of Biogenic Defense Phytohormone Salicylic Acid in Living Cells and Plants Using a Novel and Viable Rhodamine-Functionalized Fluorescent Probe

Lin-Lin Yang, Si-Yan Zou, Yi-Hong Fu, Wen Li, Xiao-Peng Wen, Pei-Yi Wang,* Zhen-Chao Wang, Gui-Ping Ouyang, Zhong Li, and Song Yang*

Cite This: https://dx.doi.org/10.1021/acs.jafc.9b06771 Read Online

ACCESS | Metrics & More | Article Recommendations | Supporting Information

ABSTRACT: Detecting plant-derived signal molecules using fluorescent probes is a key topic and a huge challenge for scientists. Salicylic acid (SA), a vital plant-derived defense hormone, can activate global transcriptional reprogramming to systemically express a network of prominent pathogenesis-related proteins against invasive microorganisms. This strategy is called systemic acquired resistance (SAR). Therefore, monitoring the dynamic fluctuations of SA in subcellular microenvironments can advance our understanding of different physiological and pathological functions during the SA-induced SAR mechanism, thus benefiting the discovery and development of novel immune activators that contribute to crop protection. Here, detection of signaling molecule SA in plant callus tissues was first reported and conducted by a simple non-fluorescent rhodamine-tagged architecture bearing a flexible 2-amino-*N*,*N*-dimethylacetamide pattern. This study can markedly advance and promote the usage of fluorescent SA probes for distinguishing SA in the plant kingdom.

KEYWORDS: *salicylic acid, systemic acquired resistance, rhodamine probe, plant callus tissues*

INTRODUCTION

Biogenic signal molecules are attractive and important physiological activators that can conduct and determine diverse physiological processes, such as cellular homeostasis, metabolism, energy conversion, signal conduction, and immunity, throughout the cell cycle.[1−6] The abnormal expression level of these bioactive substances can result in a series of imbalance and reverse effects and is constantly associated with various major diseases. Thus, detecting these biogenic signal molecules in subcellular microenvironments is crucial for bioanalysis, biomedicine, immunology, and related drug discovery. In the past few decades, numerous animal-derived bioactive ingredients, including reactive oxygen species (H_2O_2, $^1O_2$, and HOCl),[7−10] reactive sulfur species (H_2S, SO_2, GSH, and Cys),[11−15] reactive nitrogen species (HNO, NO, and NO_2),[7,16−18] acetylcholine (Ach),[19−21] adenosine triphosphate (ATP),[22−24] dopamine,[19,25−27] and histamine,[19,28−30] have been elaborately monitored by exploiting fluorescent imaging techniques. This process has achieved an improved understanding of various pathological and physiological processes that potentially benefit diagnosis and treatment of animal diseases. However, detecting plant-derived signal molecules using fluorescent probes is also a key topic and a huge challenge for scientists. Salicylic acid (SA), a vital plant-derived defensive signal molecule, can activate global transcriptional reprogramming to express a network of prominent pathogenesis-related proteins in uninoculated tissues against secondary infections from invasive microorganisms systemically.[31,32] This resistance can spontaneously spread throughout tissues of the whole plant; this mechanism is called systemic acquired resistance (SAR).[33−35] Through this process, the plant can obtain long-term protection in response to pathogen challenges controlled by the innate immune system of the plant. This process is considered the most economical and ideal strategy for crop protection. Many proofs show that the expression level of endogenous SA is enhanced in local and systemic tissues after the initial invasion of offensive pathogens, thus leading to the launch of SA-triggered signaling pathways.[32,36−38] Therefore, monitoring the dynamic fluctuations of SA in subcellular microenvironments can advance our understanding of different physiological and pathological functions during the SA-induced SAR mechanism and benefit the discovery and development of novel immune activators that contribute to crop protection. This outcome will not only secure agricultural production and food supply but also provide an ideal approach to reducing the usage of traditionally harmful pesticides, thereby eliciting the concern of people. However, the accurate, dynamic, and real-time detection of SA has achieved considerable challenges for technological restraints and significant interferences from SA analogues. These distractors are methyl salicylate, 4-hydroxybenzoic acid, 2-methylbenzoic acid, 3-hydroxybenzoic acid, benzoic acid, and catechol; thus, few chemosensors can monitor SA *in*

Received: October 28, 2019
Revised: February 4, 2020
Accepted: March 31, 2020
Published: March 31, 2020

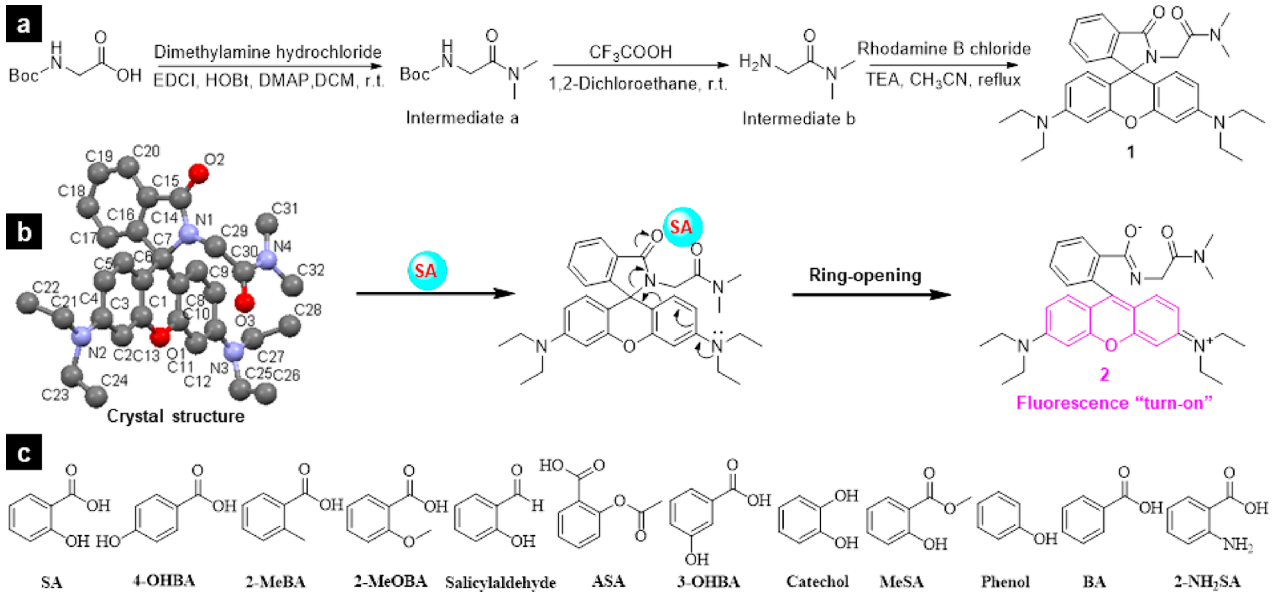

Figure 1. (a) Synthetic route for probe **1**, (b) proposed mechanism for sensing SA using probe **1**, and (c) chemical structures of SA analogues.

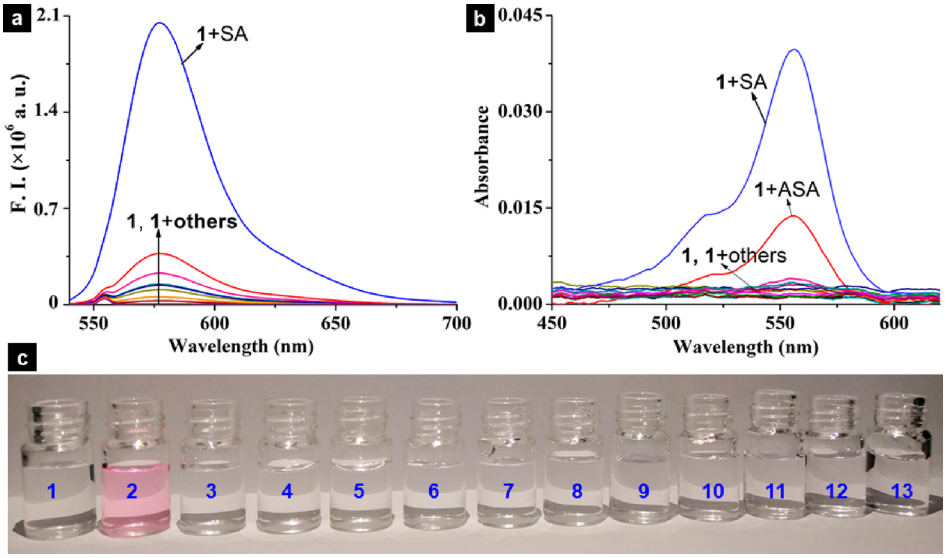

Figure 2. (a) Fluorescence and (b) absorption spectra of probe **1** (10 μM) after adding 100 μM SA and its analogues, with λ_{ex} = 554 nm, slits of 2/2 nm, and MeOH−H_2O (9:1, v/v), and (c) photographs of probe **1** (10 μM) after adding 20 equiv of SA or its analogues: (1) **1**, (2) **1** + SA, (3) **1** + 4-OHBA, (4) **1** + 2-MeBA, (5) **1** + 2-MeOBA, (6) **1** + salicylaldehyde, (7) **1** + ASA, (8) **1** + 3-OHBA, (9) **1** + catechol, (10) **1** + MeSA, (11) **1** + phenol, (12) **1** + BA, and (13) **1** + 2-NH_2BA in MeOH−H_2O (9:1, v/v).

vitro[39−43] and *in vivo*.[44] Thus, a campaign to discover and develop fluorescent probes is urgently required to monitor biological signaling molecule SA *in situ* and *in vivo*.

Rhodamine-based chemosensors, which exhibit versatile and broad detection windows, have been extensively studied and exploited for biological imaging in subcellular microenvironments.[7,18,45−47] Numerous research results have revealed that fluorescent probes containing rhodamine skeletons display exhilarating privileges, such as excellent sensitivity and selectivity,[48−51] real-time detection feature,[52−54] and low detection limits,[55,56] toward detected objects. In our previous work, a rhodamine-based sensor owning a *N*,*N*-dimethylhydrazinecarboxamide moiety could monitor SA in living animal cells.[44] To pursue a high-performing probe and further explore the substantial application in detecting SA on plants, herein, a simple and non-fluorescent rhodamine derivative **1** bearing a flexible 2-amino-*N*,*N*-dimethylacetamide pattern was rationally fabricated to monitor SA *in vitro*, in living cells and plant callus tissues (Figure 1a). Within this framework, a free-rotated methylene bridging linker was introduced to facilitate the formation of a **1**−SA binary complex in a relatively relaxed pocket promoted by hydrogen bonding. The newly formed combinations led to rearranging the electronic property of the whole molecule and subsequently caused the ring opening of the spirolactam structure accompanied by producing fluorescence for distinguishing SA (Figure 1b). An achromatous solution containing probe **1** immediately changed into pink after adding SA, thus revealing that a colorimetric probe for sensing SA with a naked-eye detection characteristic should be developed.

https://dx.doi.org/10.1021/acs.jafc.9b06771
J. Agric. Food Chem. XXXX, XXX, XXX−XXX

MATERIALS AND METHODS

Instruments and Chemicals. All chemical reagents and analytical reagent (AR) solvents were acquired from commercial suppliers and used without further purification. Distilled water was used throughout. Nuclear magnetic resonance (NMR) spectra were obtained using a JEOL-ECX 500NMR spectrometer. High-resolution mass spectroscopy (HRMS) spectra were performed on a Thermo Scientific Q Exactive mass spectrometer. Fluorescence spectra were performed by a Fluoromax-4 spectrofluorometer. Ultraviolet−visible (UV−vis) spectra were recorded by a TU-1900 spectrophotometer (Beijing Purkinje General Instrument Co., China). Fluorescence imaging was performed using a Nikon ECLIPSE Ti-S fluorescence microscope.

The stock solution of probe **1** (1.0×10^{-3} M) was prepared in methanol. Analyte stock solutions (1.0×10^{-2} M) of SA and its distractors were prepared in methanol, respectively. The preparation of samples for UV−vis and fluorescence detections follows the operations: 0.1 mL of stock solution of probe **1** was added to a 10 mL volumetric flask, and then certain amounts of detection objects were added; the mixture was filled up to 10 mL with the associated solvents; and finally, the related spectra were obtained after incubating the mixture for 10 min.

RESULTS AND DISCUSSION

Rhodamine-based chemosensor **1** was prepared, as illustrated in Figure 1a. The starting material Boc-glycine was reacted with dimethylamine through typical condensation to provide an intermediate a, which was then treated with trifluoroacetic acid to remove the protective group (−Boc) to realize an intermediate b. Finally, the target probe **1** was fabricated through a simple cyclization reaction between the intermediate b and rhodamine B chloride. The final molecular framework was confirmed using ^{1}H and ^{13}C NMR, HRMS, and its related crystal structures (Figures S1−S6 and Table S1 of the Supporting Information). Fluorescence and UV−vis spectra were performed to evaluate the detection competence of probe **1** toward SA and its distractors (Figure 1c and panels a and b of Figure 2). A methanol solvent and a methanol−water solution (9:1, v/v) were rationally selected for monitoring SA based on the fluorescence enhancement folds at 578 nm upon exposing the **1**−SA complex in various test fluids (Figures S7 and S8 of the Supporting Information). Probe **1** displayed superior selectivity and sensitivity to those of other SA analogues in detecting SA from the fluorescence spectrum (Figure 2a). These SA analogues included 4-hydroxybenzoic acid, *o*-methylbenzoic acid, *o*-methoxybenzoic acid, salicylaldehyde, acetylsalicylic acid (ASA), 3-hydroxybenzoic acid, catechol, methyl salicylate, benzoic acid, and anthranilic acid. The significantly produced fluorescent intensity triggered by adding SA revealed that SA can ring open the spirolactam pattern probably promoted by hydrogen-bonding interactions. This result was consistent with the newly generated UV absorption peak depicted in Figure 2b, thereby confirming that probe **1** can distinctively monitor SA. A pink color was only observed after adding SA (Figure 2c), thus suggesting that a colorimetric sensor was unexpectedly acquired for distinguishing SA with a naked-eye detection feature. Definitively, probe **1** showed improved detection behavior compared to our previously reported probe (Figure S9 of the Supporting Information).

To validate the selectivity and anti-interference functions further, competition assays should be conducted by subsequently adding SA to the premixed solution containing probe **1** with diverse interfering ingredients. Fluorescent intensity at 578 nm was substantially elevated only by the subsequent stimulation from SA, thus manifesting that the designed probe **1** possesses a superior anti-interference characteristic for recognizing SA (Figure 3). Moreover, a 1:1 binding

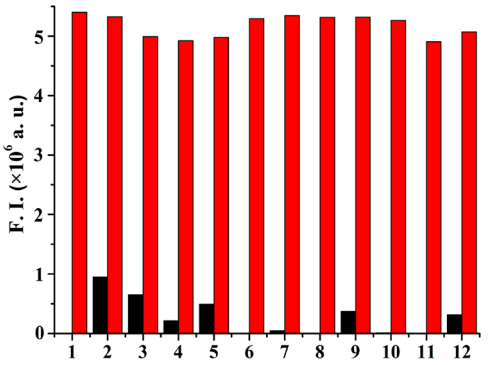

Figure 3. Competition experiments for adding 600 μM SA into the premixed solution consisting of probe **1** (10 μM) and various SA analogues (600 μM): (1) blank, (2) ASA, (3) 2-MeOBA, (4) 4-OHBA, (5) 2-MeBA, (6) catechol, (7) 2-NH_2BA, (8) MeSA, (9) BA, (10) phenol, (11) salicylaldehyde, and (12) 3-OHBA. Black bars, fluorescence intensity for probe **1** with SA analogues at 578 nm; red bars, after adding SA into the premixed solution containing probe **1** with SA analogues. Experimental conditions: λ_{ex}, 554 nm; slits, 2/2 nm; and MeOH−H_2O, 9:1 (v/v).

stoichiometry between probe **1** and SA was revealed by Job's plot experiment (Figure S10 of the Supporting Information), and the binding constant was calculated as 4.31×10^3 μM^{-1} (Figure S11 of the Supporting Information). The concentration-dependent titration assay demonstrated that the fluorescent intensity at 578 nm increases gradually after adding different dosages of SA. Consequently, a favorable linear detection within 10−100 μM was detected for a potential quantitative study (Figures S12 and S13 of the Supporting Information). Furthermore, the related detection limit was obtained as 1.0 nM by testing the signal-to-noise ratio. Given the above-mentioned results, a prospective probe that can selectively monitor SA *in vitro* in a naked-eye detection manner was discovered.

^{1}H NMR spectra were performed to explain the possible mechanism for monitoring SA in a concentration-dependent manner (Figure 4). The protons (1′, 2′, 3′, and 4′) that belong to the benzene ring of SA exhibited large chemical shifts to high fields because the molar ratio was 1:1 (Tables S2 and S3 of the Supporting Information). In contrast, further increasing the amount of SA (2 or 3 equiv) resulted in a reduced variation on the chemical shift, as illustrated by the corresponding changes in protons 1′, 2′, 3′, and 4′: −0.03, −0.08, −0.05, and −0.06 ppm for 1 equiv of SA and −0.02, −0.06, −0.04, and −0.05 ppm for 3 equiv of SA. This phenomenon might contribute to insufficient binding sites offered by probe **1** with excess SA molecules directed by hydrogen bonding. In contrast, the protons in probe **1** provided gradually increased chemical shifts by elevating the abundance of SA. The protons (11) of the methylene group showed significant low-field shifts with the changed values of 0.08 ppm for 1 equiv of SA, 0.11 for 2 equiv of SA, and 0.13 ppm for 3 equiv of SA. This finding might be due to the increased shielding effect from excess SA molecules promoted by hydrogen bonding. This action simultaneously led to rearranging the global electrons of probe **1**. The protons at the 5−10 positions presented

https://dx.doi.org/10.1021/acs.jafc.9b06771
J. Agric. Food Chem. XXXX, XXX, XXX−XXX

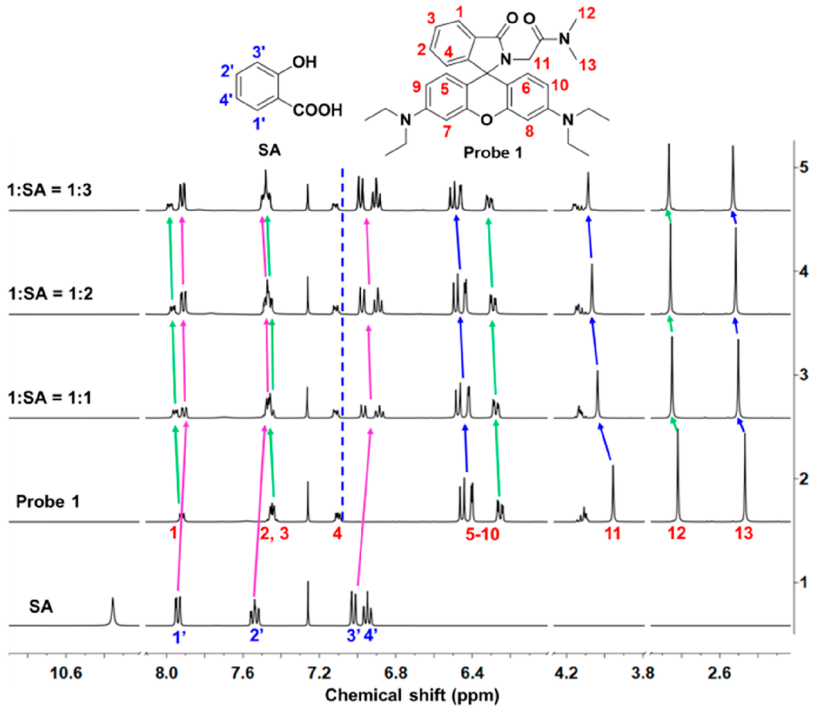

Figure 4. Partial ^{1}H NMR spectra for different molar ratios of probe **1** with SA (500 MHz, $CDCl_3$).

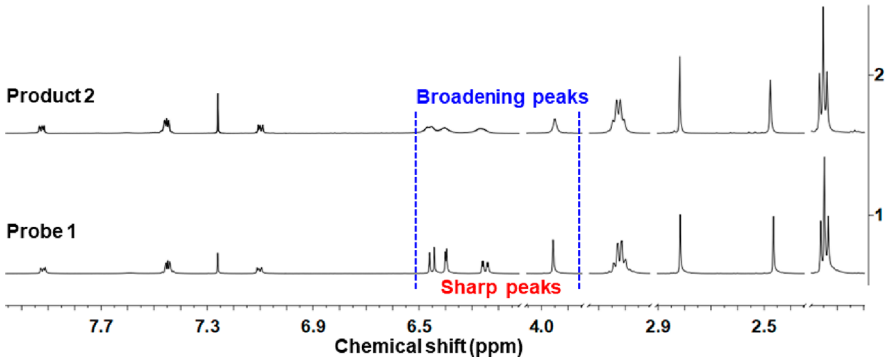

Figure 5. Comparison of partial ^{1}H NMR spectra of the new product **2** and probe **1** (500 MHz, $CDCl_3$).

considerable low-field shifts, which might be attributed to the launch of ring opening the spirolactam structure. We successfully obtained the newly fluorescent product **2** by the common separation on a silica gel column, and its molecular structure was confirmed by ^{1}H NMR and HRMS (Figure 5 and Figures S14 and S15 of the Supporting Information), in which broadening peaks were observed at 5−10 and 11 positions in comparison to those of probe **1** with sharp peaks. This finding further verified that SA detection was based on a fluorescence "turn-on" mode, thereby verifying the proposed mechanism (Figure 1b).

To explore the *in vivo* detection capability of probe **1** toward SA, A549 cell lines and plant callus tissues of *Malus asiatica* Nakai were randomly selected for SA imaging. For animal cell imaging, 10 μM probe **1** was added to the prepared A549 cells and incubated for 0.5 h at 37 °C. These cells were washed by a phosphate-buffered saline (PBS) buffer (0.01 M, pH 7.4) thrice and subsequently treated with 100 μM SA for 1 h at 37 °C. Finally, the cells were washed with PBS buffer thrice before imaging. Red fluorescent cells (Figure 6) were only observed by incubating the cells with probe **1** and SA, thereby indicating

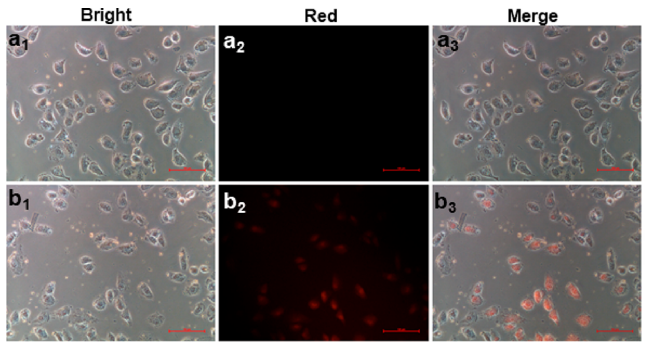

Figure 6. Fluorescence imaging of probe **1** relative to SA in living A549 cells: (a_1) bright field and (a_2) fluorescence images of A549 cells incubated using 10 μM probe **1** for 30 min at 37 °C, (a_3) merged image of a_1 and a_2, (b_1) bright field and (b_2) fluorescence image of A549 cells incubated with 10 μM probe **1** and 100 μM SA for 1 h at 37 °C, and (b_3) merged image of b_1 and b_2. Red channel, 510−560 nm.

that probe **1** could penetrate the cell membrane and detect SA in animal cells. Moreover, we found that probe **1** showed low

https://dx.doi.org/10.1021/acs.jafc.9b06771
J. Agric. Food Chem. XXXX, XXX, XXX−XXX

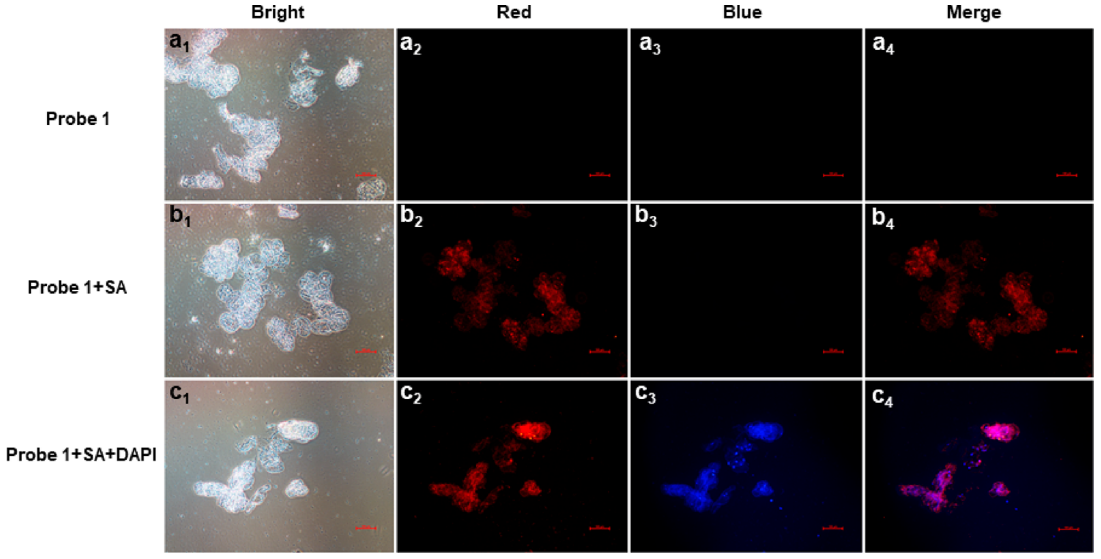

Figure 7. Fluorescence imaging of probe **1** relative to SA in living *M. asiatica* Nakai callus: (a_1) bright field and (a_2 and a_3) fluorescence images of callus tissues incubated using 10 μM probe **1** for 25 days at 25 °C, (a_4) merged image of a_2 and a_3, (b_1) bright field and (b_2 and b_3) fluorescence images of callus tissues incubated using 10 μM probe **1** and 100 μM SA for 30 days at 25 °C, (b_4) merged image of b_2 and b_3, (c_1) bright field and (c_2 and c_3) fluorescence images of callus tissues incubated with 10 μM probe **1** and 100 μM SA for 30 days at 25 °C, and (c_4) merged image of c_2 and c_3. Red channel, 510−560 nm; blue channel, 330−380 nm.

toxicity toward A549 cells monitored by 3-(4,5-dimethylthiazol-2-yl)-2,5-diphenyltetrazolium bromide (MTT) assays (Figure S16 of the Supporting Information). For plant callus tissue imaging, the corresponding incubation time for probe **1** (10 μM) and SA (100 μM) in solid agar medium was 25 and 30 days before imaging. A strongly emerging fluorescence located at callus tissues (Figure 7) was only presented in the samples containing probe **1** and SA, thereby further confirming that probe **1** can also monitor SA in plant callus tissues (Figure 7b). Moreover, the localization of coloring was mainly in the cytoplasm (Figure 7c). Thus, probe **1**, which possesses promising applications in SA signaling *in vitro* and *in vivo*, should be further developed.

In summary, a novel non-fluorescent rhodamine derivative **1** possessing a flexible 2-amino-*N*,*N*-dimethylacetamide pattern was designed and prepared to monitor SA. During this process, a probable mechanism for detecting SA was recommended. A binary complex **1**−SA could form directed by hydrogen-bonding interaction and subsequently rearranging the electronic property of the whole molecule. This occurrence would cause the ring opening of the spirolactam structure along with producing fluorescence for distinguishing SA. This outcome was further confirmed by fluorescence, UV−vis, and ^{1}H NMR spectra. The results showed that probe **1** can selectively distinguish SA *in vitro* with the detection limit of 1 nM. A favorable linear detection ranging from 10 to 100 μM was obtained for the potential quantitative study of SA. Probe **1** could be exploited to detect SA in living cells and plant callus tissues sensitively. Given these promising performances and applications, we anticipate that this probe should be further studied in monitoring SA in the plant kingdom and can launch the discovery of fresh immune activators for crop protection.

■ ASSOCIATED CONTENT

Supporting Information

The Supporting Information is available free of charge at https://pubs.acs.org/doi/10.1021/acs.jafc.9b06771.

Preparation of the intermediates and probe **1**, NMR and HRMS spectra, Tables S1−S3, and Figures S1−S16 (PDF)

■ AUTHOR INFORMATION

Corresponding Authors

Pei-Yi Wang − *State Key Laboratory Breeding Base of Green Pesticide and Agricultural Bioengineering, Key Laboratory of Green Pesticide and Agricultural Bioengineering, Ministry of Education, Center for R&D of Fine Chemicals of Guizhou University, Guiyang, Guizhou 550025, People's Republic of China;* orcid.org/0000-0002-9904-0664; Email: pywang888@126.com

Song Yang − *State Key Laboratory Breeding Base of Green Pesticide and Agricultural Bioengineering, Key Laboratory of Green Pesticide and Agricultural Bioengineering, Ministry of Education, Center for R&D of Fine Chemicals of Guizhou University, Guiyang, Guizhou 550025, People's Republic of China; College of Pharmacy, East China University of Science and Technology, Shanghai 200237, People's Republic of China;* orcid.org/0000-0003-1301-3030; Email: jhzx.msm@gmail.com

Authors

Lin-Lin Yang − *State Key Laboratory Breeding Base of Green Pesticide and Agricultural Bioengineering, Key Laboratory of Green Pesticide and Agricultural Bioengineering, Ministry of Education, Center for R&D of Fine Chemicals of Guizhou University, Guiyang, Guizhou 550025, People's Republic of China*

Si-Yan Zou − *Key Laboratory of Plant Resource Conservation and Germplasm Innovation in Mountainous Region (Ministry of Education), Institute of Agro-bioengineering/College of Life Science, Guizhou University, Guiyang, Guizhou 550025, People's Republic of China*

Yi-Hong Fu − *College of Pharmacy, Guizhou University, Guiyang, Guizhou 550025, People's Republic of China*

https://dx.doi.org/10.1021/acs.jafc.9b06771
J. Agric. Food Chem. XXXX, XXX, XXX−XXX

Wen Li − *College of Pharmacy, Guizhou University, Guiyang, Guizhou 550025, People's Republic of China*
Xiao-Peng Wen − *Key Laboratory of Plant Resource Conservation and Germplasm Innovation in Mountainous Region (Ministry of Education), Institute of Agro-bioengineering/College of Life Science, Guizhou University, Guiyang, Guizhou 550025, People's Republic of China*
Zhen-Chao Wang − *College of Pharmacy, Guizhou University, Guiyang, Guizhou 550025, People's Republic of China*
Gui-Ping Ouyang − *State Key Laboratory Breeding Base of Green Pesticide and Agricultural Bioengineering, Key Laboratory of Green Pesticide and Agricultural Bioengineering, Ministry of Education, Center for R&D of Fine Chemicals of Guizhou University, Guiyang, Guizhou 550025, People's Republic of China; College of Pharmacy, Guizhou University, Guiyang, Guizhou 550025, People's Republic of China*
Zhong Li − *College of Pharmacy, East China University of Science and Technology, Shanghai 200237, People's Republic of China*

Complete contact information is available at: https://pubs.acs.org/10.1021/acs.jafc.9b06771

Funding

The authors acknowledge funds from the National Natural Science Foundation of China (21877021, 31860516, 21702037, and 21662009), the Research Project of Ministry of Education (213033A and 20135201110005), and the Guizhou Provincial S&T Program ([2017]5788 and LH[2017]7259).

Notes

The authors declare no competing financial interest.

REFERENCES

(1) Greene, L. E.; Lincoln, R.; Cosa, G. Rate of lipid peroxyl radical production during cellular homeostasis unraveled via fluorescence imaging. *J. Am. Chem. Soc.* **2017**, *139*, 15801−15811.
(2) Zhou, X.; Zhang, K.; Qi, W.; Zhou, Y.; Hong, T.; Xiong, T.; Xie, M.; Nie, S. Exopolysaccharides from *Lactobacillus plantarum* NCU116 Enhances Colonic Mucosal Homeostasis by Controlling Epithelial Cell Differentiation and c-Jun/Muc2 Signaling. *J. Agric. Food Chem.* **2019**, *67*, 9831−9839.
(3) Yang, X.; Liu, W.; Tang, J.; Li, P.; Weng, H.; Ye, Y.; Xian, M.; Tang, B.; Zhao, Y. A multi-signal mitochondria-targeted fluorescent probe for real-time visualization of cysteine metabolism in living cells and animals. *Chem. Commun.* **2018**, *54*, 11387−11390.
(4) Niyogi, K. K.; Grossman, A. R.; Björkman, O. Arabidopsis mutants define a central role for the xanthophyll cycle in the regulation of photosynthetic energy conversion. *Plant Cell* **1998**, *10*, 1121−1134.
(5) Li, Z.; Peers, G.; Dent, R. M.; Bai, Y.; Yang, S. Y.; Apel, W.; Leonelli, L.; Niyogi, K. K. Evolution of an atypical de-epoxidase for photoprotection in the green lineage. *Nat. Plants* **2016**, *2*, 16140.
(6) Spoel, S. H.; Dong, X. How do plants achieve immunity? Defence without specialized immune cells. *Nat. Rev. Immunol.* **2012**, *12*, 89.
(7) Chen, X.; Tian, X.; Shin, I.; Yoon, J. Fluorescent and luminescent probes for detection of reactive oxygen and nitrogen species. *Chem. Soc. Rev.* **2011**, *40*, 4783−4804.
(8) Yang, B.; Chen, Y.; Shi, J. Reactive Oxygen Species (ROS)-Based Nanomedicine. *Chem. Rev.* **2019**, *119*, 4881−4985.
(9) Gao, P.; Pan, W.; Li, N.; Tang, B. Fluorescent probes for organelle-targeted bioactive species imaging. *Chem. Sci.* **2019**, *10*, 6035−6071.
(10) Chuang, C. Y.; Liu, H. C.; Wu, L. C.; Chen, C. Y.; Chang, J. T.; Hsu, S. L. Gallic Acid Induces Apoptosis of Lung Fibroblasts via a Reactive Oxygen Species-Dependent Ataxia Telangiectasia Mutated-p53 Activation Pathway. *J. Agric. Food Chem.* **2010**, *58*, 2943−2951.
(11) Chen, X.; Zhou, Y.; Peng, X.; Yoon, J. Fluorescent and colorimetric probes for detection of thiols. *Chem. Soc. Rev.* **2010**, *39*, 2120−2135.
(12) Liu, C.; Chen, W.; Shi, W.; Peng, B.; Zhao, Y.; Ma, H.; Xian, M. Rational design and bioimaging applications of highly selective fluorescence probes for hydrogen polysulfides. *J. Am. Chem. Soc.* **2014**, *136*, 7257−7260.
(13) Lin, V. S.; Chen, W.; Xian, M.; Chang, C. J. Chemical probes for molecular imaging and detection of hydrogen sulfide and reactive sulfur species in biological systems. *Chem. Soc. Rev.* **2015**, *44*, 4596−4618.
(14) He, L.; Yang, X.; Xu, K.; Kong, X.; Lin, W. A multi-signal fluorescent probe for simultaneously distinguishing and sequentially sensing cysteine/homocysteine, glutathione, and hydrogen sulfide in living cells. *Chem. Sci.* **2017**, *8*, 6257−6265.
(15) Yuan, L.; Lin, W.; Yang, Y. A ratiometric fluorescent probe for specific detection of cysteine over homocysteine and glutathione based on the drastic distinction in the kinetic profiles. *Chem. Commun.* **2011**, *47*, 6275−6277.
(16) Mao, Z.; Feng, W.; Li, Z.; Zeng, L.; Lv, W.; Liu, Z. NIR in, far-red out: Developing a two-photon fluorescent probe for tracking nitric oxide in deep tissue. *Chem. Sci.* **2016**, *7*, 5230−5235.
(17) Mao, G. J.; Zhang, X. B.; Shi, X. L.; Liu, H. W.; Wu, Y. X.; Zhou, L. Y.; Tan, W.; Yu, R. Q. A highly sensitive and reductant-resistant fluorescent probe for nitroxyl in aqueous solution and serum. *Chem. Commun.* **2014**, *50*, 5790−5792.
(18) Chen, X.; Wang, F.; Hyun, J. Y.; Wei, T.; Qiang, J.; Ren, X.; Shin, I.; Yoon, J. Recent progress in the development of fluorescent, luminescent and colorimetric probes for detection of reactive oxygen and nitrogen species. *Chem. Soc. Rev.* **2016**, *45*, 2976−3016.
(19) Pradhan, T.; Jung, H. S.; Jang, J. H.; Kim, T. W.; Kang, C.; Kim, J. S. Chemical sensing of neurotransmitters. *Chem. Soc. Rev.* **2014**, *43*, 4684−4713.
(20) Wang, C. I.; Chen, W. T.; Chang, H. T. Enzyme mimics of Au/Ag nanoparticles for fluorescent detection of acetylcholine. *Anal. Chem.* **2012**, *84*, 9706−9712.
(21) Korbakov, N.; Timmerman, P.; Lidich, N.; Urbach, B.; Sa'ar, A.; Yitzchaik, S. Acetylcholine detection at micromolar concentrations with the use of an artificial receptor-based fluorescence switch. *Langmuir* **2008**, *24*, 2580−2587.
(22) Chen, Z.; Wu, P.; Cong, R.; Xu, N.; Tan, Y.; Tan, C.; Jiang, Y. Sensitive conjugated-polymer-based fluorescent ATP probes and their application in cell imaging. *ACS Appl. Mater. Interfaces* **2016**, *8*, 3567−3574.
(23) Matsui, Y.; Funato, Y.; Imamura, H.; Miki, H.; Mizukami, S.; Kikuchi, K. Visualization of long-term Mg^{2+} dynamics in apoptotic cells using a novel targetable fluorescent probe. *Chem. Sci.* **2017**, *8*, 8255−8264.
(24) Tan, K. Y.; Li, C. Y.; Li, Y. F.; Fei, J.; Yang, B.; Fu, Y. J.; Li, F. Real-time monitoring ATP in mitochondrion of living cells: A specific fluorescent probe for ATP by dual recognition sites. *Anal. Chem.* **2017**, *89*, 1749−1756.
(25) Lin, V. S. Y.; Lai, C. Y.; Huang, J.; Song, S. A.; Xu, S. Molecular recognition inside of multifunctionalized mesoporous silicas: Toward selective fluorescence detection of dopamine and glucosamine. *J. Am. Chem. Soc.* **2001**, *123*, 11510−11511.
(26) Secor, K. E.; Glass, T. E. Selective amine recognition: Development of a chemosensor for dopamine and norepinephrine. *Org. Lett.* **2004**, *6*, 3727−3730.
(27) Reviriego, F.; Navarro, P.; García-España, E.; Albelda, M. T.; Frías, J. C.; Domènech, A.; Yunta, M. J. R.; Costa, R.; Ortí, E. Diazatetraester 1*H*-pyrazole crowns as fluorescent chemosensors for AMPH, METH, MDMA (ecstasy), and dopamine. *Org. Lett.* **2008**, *10*, 5099−5102.
(28) Oshikawa, Y.; Furuta, K.; Tanaka, S.; Ojida, A. Cell surface-anchored fluorescent probe capable of real-time imaging of single

mast cell degranulation based on histamine-induced coordination displacement. *Anal. Chem.* **2016**, *88*, 1526−1529.
(29) Seto, D.; Soh, N.; Nakano, K.; Imato, T. An amphiphilic fluorescent probe for the visualization of histamine in living cells. *Bioorg. Med. Chem. Lett.* **2010**, *20*, 6708−6711.
(30) Kielland, N.; Vendrell, M.; Lavilla, R.; Chang, Y. T. Imaging histamine in live basophils and macrophages with a fluorescent mesoionic acid fluoride. *Chem. Commun.* **2012**, *48*, 7401−7403.
(31) van Loon, L. C.; Rep, M.; Pieterse, C. M. J. Significance of inducible defense-related proteins in infected plants. *Annu. Rev. Phytopathol.* **2006**, *44*, 135−162.
(32) Kachroo, A.; Robin, G. P. Systemic signaling during plant defense. *Curr. Opin. Plant Biol.* **2013**, *16*, 527−533.
(33) Durrant, W. E.; Dong, X. Systemic acquired resistance. *Annu. Rev. Phytopathol.* **2004**, *42*, 185−209.
(34) Chisholm, S. T.; Coaker, G.; Day, B.; Staskawicz, B. J. Host−microbe interactions: Shaping the evolution of the plant immune response. *Cell* **2006**, *124*, 803−814.
(35) Jones, J. D.; Dangl, J. L. The plant immune system. *Nature* **2006**, *444*, 323.
(36) Mou, Z.; Fan, W.; Dong, X. Inducers of plant systemic acquired resistance regulate NPR1 function through redox changes. *Cell* **2003**, *113*, 935−944.
(37) Wang, D.; Weaver, N. D.; Kesarwani, M.; Dong, X. Induction of protein secretory pathway is required for systemic acquired resistance. *Science* **2005**, *308*, 1036−1040.
(38) Gust, A. A.; Nürnberger, T. Plant immunology: A life or death switch. *Nature* **2012**, *486*, 198.
(39) Ahmad, M. W.; Kim, B. Y.; Kim, H. S. Selective fluorescence sensing of salicylic acid using a simple pyrene appended imidazole receptor. *New J. Chem.* **2014**, *38*, 1711−1716.
(40) Salinas, F.; de La Peña, A. M.; Durán-Merás, I.; Durán, M. S. Determination of salicylic acid and its metabolites in urine by derivative synchronous spectrofluorimetry. *Analyst* **1990**, *115*, 1007−1011.
(41) Kumar, A.; Ghosh, M. K.; Choi, C. H.; Kim, H. S. Selective fluorescence sensing of salicylic acids using a simple pyrenesulfonamide receptor. *RSC Adv.* **2015**, *5*, 23613−23621.
(42) Pandith, A.; Hazra, G.; Kim, H. S. A new fluorogenic sensing platform for salicylic acid derivatives based on $\pi-\pi$ and NH$-\pi$ interactions between electron -deficient and electron-rich aromatics. *Spectrochim. Acta, Part A* **2017**, *178*, 151−159.
(43) Kumar, A.; Pandith, A.; Kim, H. S. Pyrenebutylamidopropylimidazole as a multi-analyte sensor for 3,5-dinitrosalicylic acid and Hg^{2+} ions. *J. Lumin.* **2016**, *172*, 309−316.
(44) Wang, P. Y.; Luo, X.; Yang, L. L.; Zhao, Y. C.; Dong, R.; Li, Z.; Yang, S. A rhodamine-based highly specific fluorescent probe for the *in situ* and *in vivo* imaging of the biological signalling molecule salicylic acid. *Chem. Commun.* **2019**, *55*, 7691−7694.
(45) Chen, X.; Pradhan, T.; Wang, F.; Kim, J. S.; Yoon, J. Fluorescent chemosensors based on spiroring-opening of xanthenes and related derivatives. *Chem. Rev.* **2012**, *112*, 1910−1956.
(46) Li, K.; Xiang, Y.; Wang, X.; Li, J.; Hu, R.; Tong, A.; Tang, B. Z. Reversible photochromic system based on rhodamine B salicylaldehyde hydrazone metal complex. *J. Am. Chem. Soc.* **2014**, *136*, 1643−1649.
(47) Xue, Y.; Liang, W.; Li, Y.; Wu, Y.; Peng, X.; Qiu, X.; Liu, J.; Sun, R. Fluorescent pH-Sensing Probe Based on Biorefinery Wood Lignosulfonate and Its Application in Human Cancer Cell Bioimaging. *J. Agric. Food Chem.* **2016**, *64*, 9592−9600.
(48) Zhou, J.; Li, L.; Shi, W.; Gao, X.; Li, X.; Ma, H. HOCl can appear in the mitochondria of macrophages during bacterial infection as revealed by a sensitive mitochondrial-targeting fluorescent probe. *Chem. Sci.* **2015**, *6*, 4884−4888.
(49) Liu, C.; Zhang, X.; Li, Z.; Chen, Y.; Zhuang, Z.; Jia, P.; Zhu, H.; Yu, Y.; Zhu, B.; Sheng, W. Novel Dimethylhydrazine-Derived Spirolactam Fluorescent Chemodosimeter for Tracing Basal Peroxynitrite in Live Cells and Zebrafish. *J. Agric. Food Chem.* **2019**, *67*, 6407−6413.
(50) Xiang, Y.; Tong, A.; Jin, P.; Ju, Y. New fluorescent rhodamine hydrazone chemosensor for Cu(II) with high selectivity and sensitivity. *Org. Lett.* **2006**, *8*, 2863−2866.
(51) Wang, X.; Tao, J.; Chen, X.; Yang, H. An ultrasensitive and selective "off-on" rhodamine-based colorimetric and fluorescent chemodosimeter for the detection of Cu^{2+}. *Sens. Actuators, B* **2017**, *244*, 709−716.
(52) Koide, Y.; Urano, Y.; Hanaoka, K.; Terai, T.; Nagano, T. Development of an Si-rhodamine-based far-red to near-infrared fluorescence probe selective for hypochlorous acid and its applications for biological imaging. *J. Am. Chem. Soc.* **2011**, *133*, 5680−5682.
(53) Ko, S. K.; Yang, Y. K.; Tae, J.; Shin, I. In vivo monitoring of mercury ions using a rhodamine-based molecular probe. *J. Am. Chem. Soc.* **2006**, *128*, 14150−14155.
(54) Fan, L.; Wang, X.; Ge, J.; Li, F.; Zhang, C.; Lin, B.; Shuang, S.; Dong, C. A. Golgi-targeted off-on fluorescent probe for real-time monitoring of pH changes in vivo. *Chem. Commun.* **2019**, *55*, 6685−6688.
(55) Tian, X.; Tong, X.; Li, Z.; Li, D.; Kong, Q.; Yang, X. In vivo fluoride ion detection and imaging in mice using a designed near-infrared ratiometric fluorescent probe based on IR-780. *J. Agric. Food Chem.* **2018**, *66*, 11486−11491.
(56) Fang, C.; Agarwal, A.; Buddharaju, K. D.; Khalid, N. M.; Salim, S. M.; Widjaja, E.; Garland, M. V.; Balasubramanian, N.; Kwong, D. L. DNA detection using nanostructured SERS substrates with Rhodamine B as Raman label. *Biosens. Bioelectron.* **2008**, *24*, 216−221.

https://dx.doi.org/10.1021/acs.jafc.9b06771
J. Agric. Food Chem. XXXX, XXX, XXX−XXX